EPJ Web of Conferences **60**, 19003 (2013)
DOI: 10.1051/epjconf/20136019003

Measurement of diboson production with the ATLAS detector

Suen Hou[1,a], on behalf of the ATLAS collaboration

[1] *Academia Sinica, Taipei*

Abstract. ATLAS measurements of diboson production processes involving combinations of W, Z and isolated photons are summarized. Measurements using data at 7 TeV as well as more recent results using data at 8 TeV are presented. The measurements are performed using leptonic decay modes, including the invisible decay $Z \to \nu\bar{\nu}$, as well as semileptonic channels. Differential and total cross sections are presented and are used to place constraints on anomalous triple-gauge boson couplings. An overview of these results is given.

1 Introduction

The large data statistics collected by ATLAS [1] in 2011 and 2012, in LHC pp collisions at $\sqrt{s}$ = 7 TeV and 8 TeV, respectively, provide precision measurements of the diboson production mechanism described by the Electroweak sector of the Standard Model (SM). All analyses make use of leptonic decay of W and Z bosons, for diboson processes of WW, WZ, ZZ, $W\gamma$ and $Z\gamma$. The integrated luminosities of analyzed data corresponds to 4.6 fb^{-1} at $\sqrt{s}$ = 7 TeV and up to 20 fb^{-1} at $\sqrt{s}$ = 8 TeV. The production cross sections are known to next-to-leading order (NLO), and the electroweak radiation corrections are important at high $\sqrt{s}$ [2, 3]. Therefore the cross-section measurements provide sensitive tests of the electroweak interaction at the TeV scale.

Diboson channels are also sensitive to new physics phenomena, either through resonant production of new particles or through anomalous contribution to Triple Gauge couplings (TGCs). Interactions between gauge boson are predicted by the SM. Any deviation of the triple gauge couplings from the SM prediction will enhance diboson production with higher invariant masses. Studies of diboson events are candles to improve understanding of background processes in searches of SM Higgs boson and new physics at the high energy frontier.

In the following we present measurements of diboson production cross sections and searches of anomalous contributions to SM predicted triple gauge couplings.

2 Cross-section measurements

All the analyses requires leptons (electrons or muons) originated from the decay of a W or Z boson with large transverse momentum within the detector fiducial region of pseudo-rapidity $|\eta| < 2.47$ for electrons (excluding the barrel-endcap transition region of $1.36 < |\eta| < 1.52$) and $|\eta| < 2.4$ for muons. The selection criteria vary slightly on $|\eta|$ ranges and p_{T} thresholds for leptons in different diboson channels. To reject leptons from fragmentation of jets, isolation cuts are imposed. Jets are built by clustering energy depositions in the calorimeter using the anti-kT algorithm with radius parameter 0.4. The neutrino from W decay is inferred by the missing transverse energy $E_{\mathrm{T}}^{\mathrm{miss}}$ calculated using reconstructed physics objects and calorimeter energy depositions not associated to physics objects.

The measurements of diboson production cross sections in the detector fiducial region are derived with the observed events and corrections for the event selection and reconstruction efficiencies. The total cross sections of $pp \to VV$ (with $V = W, Z$) are derived with extrapolation to the full phase space and branching ratio of W and Z decay channels of the event selection. For the $V\gamma$ channels, only fiducial cross sections are measured to avoid collinear and infrared divergences. The event selection criteria of each diboson processes are described in the following. The measurements are compared to the next-to-leading order calculations of various event generators including MCFM [4] and using the CT10 [5] and MSTW [6] parton distribution functions.

2.1 $W^+W^- \to \ell^+\nu\ell'^-\nu'$ channels

The W^+W^- production cross section is measured using the full 7 TeV dataset of 4.6 fb^{-1} [7]. Only leptonic decays of both W bosons are used, leading to a final state of two leptons and large event $E_{\mathrm{T}}^{\mathrm{miss}}$. Backgrounds consist of $t\bar{t}$, W/Z + jets and other diboson processes. To distinguish the signal from the large W/Z + jets and $t\bar{t}$ backgrounds, events are required to have large missing transverse energy and no high transverse momentum jets. Resonant Z events are removed by a mass window cut of $|m_{\ell\ell'} - m_Z| > 15$ GeV.

The observed distribution of the transverse mass calculated from the two leptons and $E_{\mathrm{T}}^{\mathrm{miss}}$ is shown in Figure 1. The measured cross sections [7] are listed in Table 1, and they agree within errors with the SM NLO predictions.

[a] e-mail: suen.hou@cern.ch

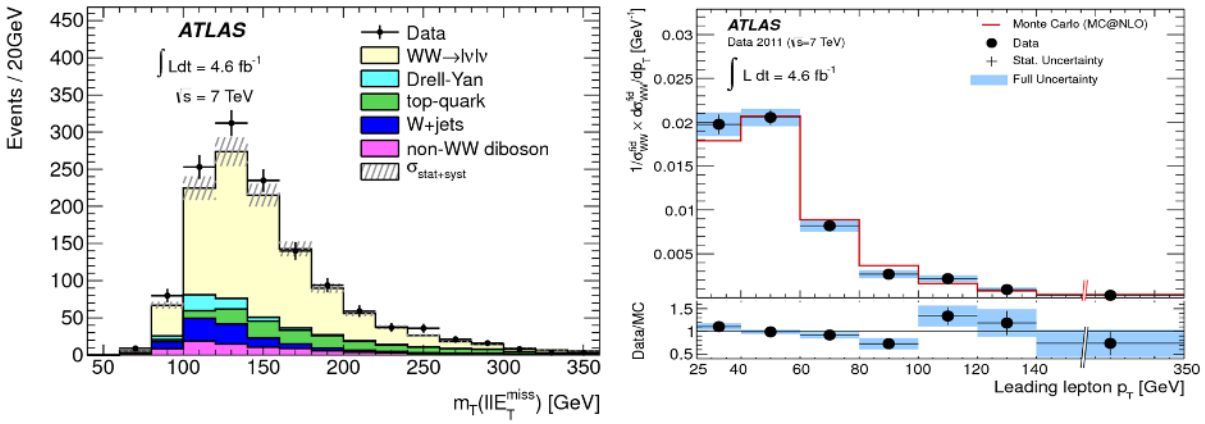

Figure 1. Distribution of transverse mass of the $\ell\ell' + E_{\mathrm{T}}^{\mathrm{miss}}$ (left) for selected WW events, and the normalized differential cross section in detector fiducial region as a function of the leading lepton p_{T} [7].

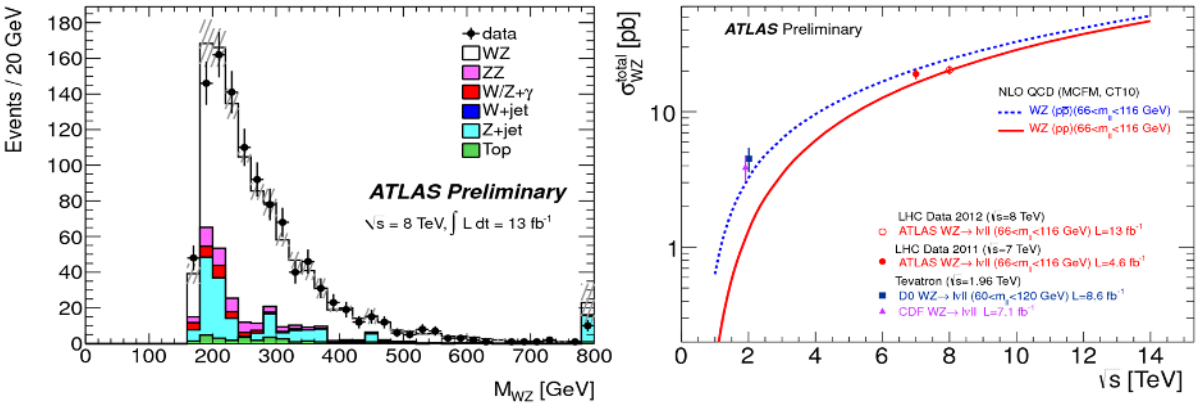

Figure 2. Distribution of the WZ invariant mass (left), using 13 fb^{-1} of $\sqrt{s} = 8$ TeV data. Measurements and theoretical predictions are plotted (right) for the total WZ production cross section as a function of center-of-mass energy [9].

The normalized differential cross section as a function of the leading lepton p_{T} is illustrated in Figure 1.

2.2 $W^{\pm}Z \to \ell^{\pm}\nu\ell'^{+}\ell'^{-}$ channels

$W^{\pm}Z$ events using leptonic decays are analyzed from the 7 TeV data (4.6 fb^{-1}) [8], and the first part of the 8 TeV data corresponding to 13 fb^{-1} [9]. The events are required to have three isolated leptons with large $E_{\mathrm{T}}^{\mathrm{miss}}$. Two leptons are required to form the Z boson with the invariant mass within 10 GeV of the Z mass. The background events include Z + jets and $t\bar{t}$. The systematic uncertainties mainly come from lepton and $E_{\mathrm{T}}^{\mathrm{miss}}$ reconstructions.

The observed $W^{\pm}Z$ transverse mass distribution of the 8 TeV data is shown in Figure 2. The measured cross sections are listed in Table 1. Comparison with the theoretical calculations are illustrated in Figure 2 for both 7 and 8 TeV data.

2.3 Semileptonic $WW, WZ \to \ell\nu jj$ channels

The measurements of semileptonic diboson production is conducted with the 7 TeV data (4.6 fb^{-1}) [10] for WW and WZ channels requiring one high-p_{T} lepton of W decay and two jets from a boson (W or Z) decay. Background is dominated by the irreducible W + jets events. The combined cross section of WW and WZ is listed in Table 1. The large systematic uncertainty is mainly due to uncertainties in the background estimation.

2.4 $ZZ \to \ell^{+}\ell^{-}\ell'^{+}\ell'^{-}, \ell^{+}\ell^{-}\nu\bar{\nu}$ channels

The ZZ production cross section is studied from 7 TeV data (4.6 fb^{-1}) [11] and the full 8 TeV data (20 fb^{-1}) [12]. Events are selected in two decay modes of $ZZ \to \ell^{+}\ell^{-}\ell'^{+}\ell'^{-}$ and $ZZ \to \ell^{+}\ell^{-}\nu\bar{\nu}$ (using 7 TeV data).

The event selection for $ZZ \to 4\ell$ requires exactly four high-p_{T} leptons, forming two opposite-sign same-flavor pairs. Ambiguities in pairing are resolved by minimizing the mass differences of the pairs to Z mass. After requiring both Z to be on-shell, with Z pair mass within $66 < m_{\ell^{+}\ell^{-}} < 116$ GeV, the candidate sample is very clean with background contribution of a few percents. Plotted in Figure 3 is the four-lepton invariant mass distribution obtained with the 8 TeV data.

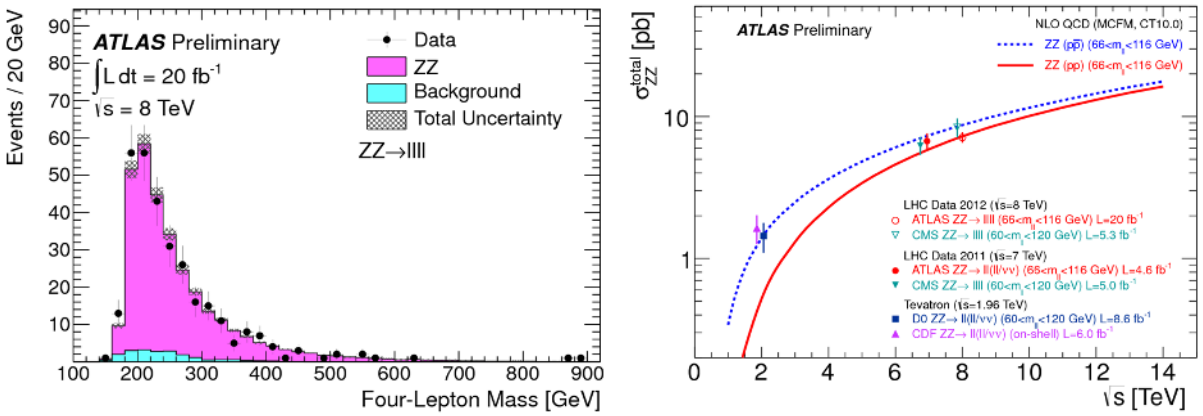

Figure 3. Invariant mass distribution for ZZ candidates (left) in leptonic decay channels using full 8 TeV data of 2012. Measurements and theoretical predictions are plotted (right) for the total ZZ production cross section as a function of center-of-mass energy [12].

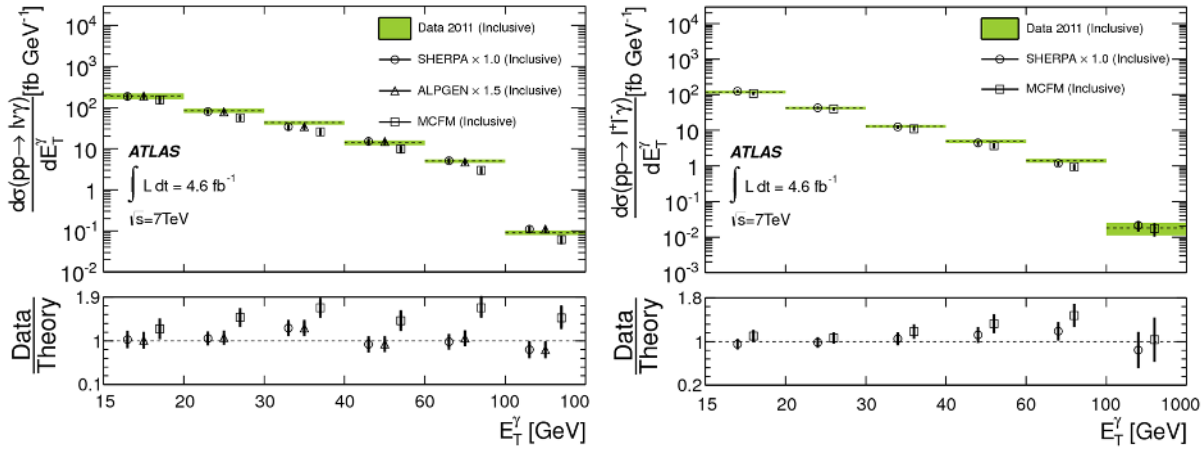

Figure 4. Differential cross sections of photon E_{T} of $W\gamma$ (left) and $Z\gamma$ (right) events. The lower plots show the ratio of the data to the predictions by different generators [13]).

The event sample for $\ell^+\ell^-\nu\bar{\nu}$ mode is selected from 7 TeV data, with two opposite-sign same-flavor leptons and large event $E_{\mathrm{T}}^{\mathrm{miss}}$. The background includes Z + jets, $t\bar{t}$ and other diboson processes. A mass window cut is required for the lepton pair. Events are further required to be without high-p_{T} jets to suppress Z+jets and $t\bar{t}$ background. The projection of $E_{\mathrm{T}}^{\mathrm{miss}}$ along p_{T}^{Z} is required to exceed 75 GeV.

The measured cross sections are listed in Table 1, for 4ℓ mode of the 8 TeV data and the combined 4ℓ and $\ell\ell\nu\bar{\nu}$ modes of the 7 TeV data. Illustrated in Figure 3 is the comparison of cross-section measurements with SM NLO calculations for both 7 and 8 TeV data. The measured cross sections are consistent within errors with the SM NLO predictions.

2.5 $W^{\pm}\gamma \to \ell^{\pm}\nu\gamma$, $Z\gamma \to \ell^+\ell^-\gamma$, $\nu\bar{\nu}\gamma$ channels

The $W^{\pm}\gamma$ and $Z\gamma$ cross sections were measured using the 7 TeV dataset corresponding to 4.6 fb^{-1} [13]. The lower energy threshold for $W\gamma$ and $Z\gamma$ implies large production cross section. Photons can be radiated from the colliding patrons or from the W boson. Additional contributions come from final state radiation (FSR) with the photon irradiated from decay leptons in W and Z events. The interference between these processes and the NLO corrections introduce large correction factor to high-p_{T} photons. Only leptonic decays of W and Z, including $Z \to \nu\bar{\nu}$ are used. To suppress FSR events, photons are required to be separated from leptons ($\Delta R(\ell,\gamma) > 0.7$). Background includes events with jet-induced photons or jet-faking leptons. Major background processes are W + jets and γ + jets for $W\gamma$, Z + jets for $Z(\to \ell\ell)\gamma$, and Z + jets, γ + jets and multijets for $Z(\to \nu\bar{\nu})\gamma$.

Events are selected in the detector fiducial phase space listed in Table 1. The $W\gamma$ sample are required to have a lepton, a photon and large $E_{\mathrm{T}}^{\mathrm{miss}}$. The selection for $Z(\to \ell\ell)\gamma$ requires a mass threshold of $m_{\ell^+\ell^-} > 40$ GeV. To suppress jet-induced background, $Z(\to \nu\bar{\nu})\gamma$ events must have a very energetic photon of $E_{\mathrm{T}} > 100$ GeV and $E_{\mathrm{T}}^{\mathrm{miss}} > 90$ GeV.

Illustrated in Figure 4 are the differential cross sections of $W(\to \ell\nu)\gamma$ and $Z(\to \ell\ell)\gamma$ as functions of the photon E_{T}, in comparison with the theoretical calculations. The cross-

Table 1. Measured diboson production cross sections in comparison with the SM NLO calculations. Cross sections of massive diboson pairs (WW, WZ, ZZ) are corrected to the full phase space. Measurements for $W\gamma$ and $Z\gamma$ are in fiducial regions as indicated.

channel	$\sqrt{s}$ (TeV)	$\int L$ (fb^{-1})	$\sigma(pp \to VV)$ (pb)	SM NLO prediction (pb)
$WW \to \ell\nu\ell'\nu'$	7	4.6	51.9 ± 2.0 (stats.) ± 3.9 (syst.) ± 2.0 (lumi.) [7]	$44.7^{+2.1}_{-1.9}$
$WZ \to \ell\nu\ell'\ell'$	7	4.6	$19.0^{+1.4}_{-1.3}$ (stat.) ± 0.9 (syst.) ± 0.4 (lumi.) [8]	$17.6^{+1.1}_{-1.0}$
	8	13	$20.3^{+0.8}_{-0.7}$ (stat.) $^{+1.2}_{-1.1}$ (syst.) $^{+0.7}_{-0.6}$ (lumi.) [9]	20.3 ± 0.8
$WW, WZ \to \ell\nu jj$	7	4.6	72 ± 9 (stat.) ± 15 (syst.) ± 13 (MC stats.) [10]	63.4 ± 2.6
$ZZ \to \ell\ell\ell'\ell', \ell\ell\nu\bar{\nu}$	7	4.6	6.7 ± 0.7 (stat.) $^{+0.4}_{-0.3}$ (syst.) ± 0.3 (lumi.) [11]	$5.89^{+0.22}_{-0.18}$
$ZZ \to \ell\ell\ell'\ell'$	8	20	$7.1^{+0.5}_{-0.4}$ (stat.) ± 0.3 (syst.) ± 0.2 (lumi.) [12]	$7.2^{+0.3}_{-0.2}$
$W\gamma \to \ell\nu\gamma$	7	4.6	$p_{\mathrm{T}}^{\ell} > 25$ GeV $\lvert\eta\rvert < 2.47$; $E_{\mathrm{T}}^{\gamma} > 15$ GeV, $\lvert\eta\rvert < 2.37$; $p_{\mathrm{T}}^{\nu} > 35$ GeV	
			2.77 ± 0.03 (stat.) ± 0.33 (syst.) ± 0.14 (lumi.) [13]	1.96 ± 0.17
$Z\gamma \to \ell\ell\gamma$	7	4.6	$p_{\mathrm{T}}^{\ell} > 25$ GeV, $\lvert\eta\rvert < 2.47$; $E_{\mathrm{T}}^{\gamma} > 15$ GeV, $\lvert\eta\rvert < 2.37$; $m(\ell\ell) > 40$ GeV	
			1.31 ± 0.02 (stat.) ± 0.11 (syst.) ± 0.05 (lumi.) [13]	1.18 ± 0.05
$Z\gamma \to \nu\bar{\nu}\gamma$	7	4.6	$p_{\mathrm{T}}^{\nu\bar{\nu}} > 90$ GeV; $E_{\mathrm{T}}^{\gamma} > 100$ GeV	
			0.133 ± 0.013 (stat.) ± 0.020 (syst.) ± 0.005 (lumi.) [13]	0.156 ± 0.012

section measurements obtained in the fiducial regions are listed in Table 1.

3 Anomalous Triple Gauge Coupling

Contributions of anomalous triple gauge couplings (aTGCs) can be parametrized by effective Lagrangian with the couplings listed in Table 2 [14, 15, 16]. In the SM, charged TGCs contribute to WW, WZ and $W\gamma$ channels, with the values of $\lambda_V = 0$ and g_1^V and κ^V equal 1. Coupling between neutral bosons (Z,γ) are not present, namely $h_i^{Z,\gamma} = f_i^{Z,\gamma} = 0$. The aTGCs are the variations of the TGCs from their SM values.

The anomalous couplings are assumed to have energy scale dependence. To avoid unitarity violation, the strength must vanish at high diboson invariant mass ($\sqrt{\hat{s}}$). A form-factor parametrization is applied to all the aTGCs with $\alpha(\hat{s}) = \alpha_0/(1 + \hat{s}/\Lambda^2)^n$, where Λ is the cut-off scale with values chosen (2 or 3 TeV), and $n = 2$, 3, or 4 depending on the coupling.

Table 2. TGC vertices, and the corresponding diboson channels and couplings in the effective Lagrangians.

vertex	channels	couplings
$WW\gamma$	WW, $W\gamma$	λ_γ, $\Delta\kappa_\gamma$
WWZ	WW, WZ	λ_Z, $\Delta\kappa_Z$, Δg_1^Z
$ZZ\gamma$	$Z\gamma$	h_3^Z, h_4^Z
$Z\gamma\gamma$	$Z\gamma$	h_3^γ, h_4^γ
$Z\gamma Z$	ZZ	f_4^γ, f_5^γ
ZZZ	ZZ	f_4^Z, f_5^Z

Non-zero aTGCs are predicted to contribute excess event rates in higher invariant mass region, and thus more high-p_{T} decay secondaries than the SM predictions. The observables to be examined are the kinematic distributions of p_{T} of bosons or their decay leptons. The likelihood function calculated by comparing the p_{T} spectrum to the predictions with varying aTGCs is used to set 95% confidence interval on the aTGCs.

Illustrated in figure 5 are the 95% C.L. limits of charged aTGCs for WWZ and $WW\gamma$ vertices. Results are obtained from the WW, WZ and $W\gamma$ analyses using 7 TeV data [7, 8, 13].

W^+W^- production is sensitive to aTGCs in the $WW\gamma$ and WWZ vertices, and thus depends on all charged aTGCs. The p_{T} distribution of the leading lepton is used to derive aTGC limits for the "LEP scenario" [17] and the number of independent aTGCs is only three ($\Delta\kappa_Z$, λ_Z and Δg_1^Z). $W^{\pm}Z$ and $W\gamma$ events are sensitive to WWZ and $WW\gamma$ vertices, respectively. The $p_{\mathrm{T}}(Z)$ spectrum of WZ sample is used to derive aTGCs of WWZ, and the photon spectrum of $W\gamma$ sample is used for the two aTGCs of the $WW\gamma$ vertex.

The effective Lagrangians for ZZ and $Z\gamma$ channels differ for the different vertices. The ZZ production is sensitive to the ZZZ and $Z\gamma Z$ vertices. Using the 7 TeV data, 95% confidence intervals are set for the f_4^γ, f_5^γ f_4^Z, and f_5^Z and shown in Figure 6 [11].

The photon spectrum, particularly at high photon energies, is sensitive to the $ZZ\gamma$ and and $Z\gamma\gamma$ couplings. The 95% confidence intervals for the CP conserving couplings h_3^γ, h_4^γ, h_3^Z, and h_4^Z are presented in Figure 6 [13].

4 Summary

The diboson production cross sections are measured and are found to be consistent with the SM predictions. Data

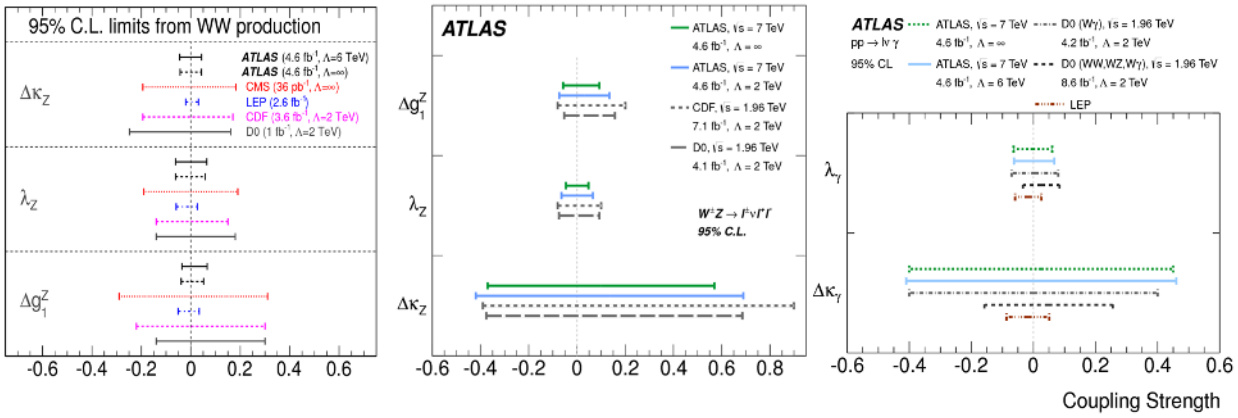

Figure 5. The 95% CL intervals for charged aTGCs in WWZ and $WW\gamma$ vertices derived from WW (left) [7], WZ (middle) [8], and $W\gamma$ (right) [13] channels.

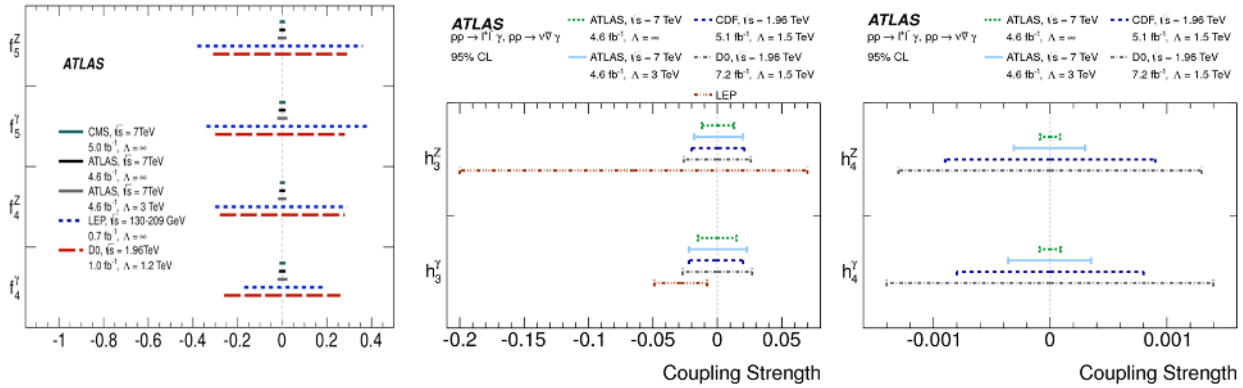

Figure 6. The 95% CL intervals for neutral aTGCs derived from data of ZZ (left) [11] and $Z\gamma$ (middle, right) [13] channels.

agree with SM predicted triple gauge couplings and 95% C.L. limits are set for the anomalous couplings.

References

[1] ATLAS Collaboration, JINST **3**, S08003 (2008).
[2] J. Ellison et al. Ann. Rev. Nucl. Part. Sci. **48** 33 (1998).
[3] M.S. Neubauer, Annu. Rev. Nucl. Part.Sci. **61**, 223 (2011), and references there in.
[4] J.M. Campbell el. al, JHEP **07** 018 (2011).
[5] H.-L. Lai et al., Phys. Rev. D **82** 074024 (2010).
[6] A. Martin et al., Eur. Phys. J. C **63** 189 (2009).
[7] ATLAS Collaboration, Phys. Rev. D **87** 112001 (2013).
[8] ATLAS Collaboration, Eur. Phys. J. C **72**:2173 (2012).
[9] ATLAS Collaboration, ATLAS-CONF-2013-021.
[10] ATLAS Collaboration, ATLAS-CONF-2012-157.
[11] ATLAS Collaboration, JHEP **03** 128 (2013).
[12] ATLAS Collaboration, ATLAS-CONF-2013-020.
[13] ATLAS Collaboration, Phys. Rev. D **87** 112003 (2013).
[14] K. Hagiwara et al., Nucl. Phys. **B282** 253 (1987).
[15] U. Baur, D. Rainwater, Phys. Rev. D **62**:113011 (2000).
[16] U. Baur, E.L. Berger, Phys. Rev. D **47**:4889 (1993).
[17] G. Gounaris et al., arXiv:hep-ph/9601233.